Title

Upscaling THM modeling from small-scale to full-scale in-situ experiments in the Callovo-Oxfordian claystone

Authors

Seyedi, DM
Plúa, C
Vitel, M
et al.

Publication Date

2021-08-01

DOI

10.1016/j.ijrmms.2020.104582

Peer reviewed

International Journal of Rock Mechanics & Mining Sciences 144 (2021) 104582

Contents lists available at ScienceDirect

International Journal of Rock Mechanics and Mining Sciences

journal homepage: www.elsevier.com/locate/ijrmms

Upscaling THM modeling from small-scale to full-scale in-situ experiments in the Callovo-Oxfordian claystone

D.M. Seyedi [a,1], C. Plúa [b,*], M. Vitel [a], G. Armand [b], J. Rutqvist [c], J. Birkholzer [c], H. Xu [c], R. Guo [d], K.E. Thatcher [e], A.E. Bond [e], W. Wang [f], T. Nagel [f,g], H. Shao [h], O. Kolditz [f,i]

[a] Andra, Châtenay-Malabry, France
[b] Andra, Meuse/Haute-Marne Underground Research Laboratory, Bure, France
[c] Lawrence Berkeley National Laboratory (LBNL), Berkeley, CA, USA
[d] Nuclear Waste Management Organization, Toronto, Canada
[e] Quintessa Ltd, Warrington, UK
[f] Helmholtz-Centre for Environmental Research, UFZ, Leipzig, Germany
[g] Freiberg University of Mining and Technology, Freiberg, Germany
[h] Federal Institute for Geosciences and Natural Resources, BGR, Hanover, Germany
[i] Dresden University of Technology (TUD), Dresden, Germany

ARTICLE INFO

Keywords:
In-situ experiments
Thermo-hydro-mechanical behavior
Callovo-oxfordian claystone
Numerical modeling
High level waste

ABSTRACT

The coupled Thermo-Hydro-Mechanical (THM) behavior of the Callovo-Oxfordian claystone (COx) is of great importance for the design and safety calculations of the high-level radioactive waste disposal project in this potential host rock in France. The heat emitted by the waste causes a pore pressure increase within the surrounding rock essentially due to the differential thermal expansion of the pore water and the solid skeleton. The low permeability of the COx and its relative rigidity inhibits the discharge of the induced pressure build-up. Moreover, thermal loading may provoke thermo-mechanical stresses within the formation due to mechanical confinement by the rigidity of the surrounding host rock. An important research program has been conducted by the French National Radioactive Waste Management Agency (Andra) since 2003 in order to investigate the THM response of the COx under thermal loading, through laboratory tests, in-situ experiments, model development and numerical modeling. Within Task E of the DECOVALEX-2019 project, five research teams investigated upscaling THM modeling from a small-scale in-situ experiment (TED) to a full-scale in-situ experiment (ALC). The upscaling modeling started with a verification test to validate the numerical codes. Then, an interpretative modeling of the TED experiment was performed to calibrate the THM parameters of the COx. Finally, the calibrated THM parameters were used for a blind prediction of the ALC experiment. The modeling teams each adopted a thermo-poro-elastic approach which yielded satisfactory results. The blind prediction of the temperature field showed an overestimation of less than 2 °C which was considered acceptable. On the other hand, pore pressure was well predicted only in the direction parallel to the bedding whereas the slow dissipation of the pore pressure in the direction perpendicular to the bedding was not captured by any of the modeling teams – which remains an open question of the present study.

1. Introduction

The Callovo-Oxfordian claystone (COx) has been selected to host the French deep geological disposal for intermediate-level long-lived and high-level radioactive waste. The COx formation lies between 420 m and 550 m in depth and presents favorable characteristics such as a very low permeability, a significant retention capacity for radionuclides, and low molecular diffusion rates.[1]

The current concept of the High Level Waste (HLW) repository in France is based on the emplacement of waste packages in 150 m long parallel micro-tunnels for the most exothermic HLW (HLW1/HLW2) and 80 m for the moderately exothermic HLW (HLW0). The latter will be

* Corresponding author.
E-mail address: carlos.plua@andra.fr (C. Plúa).
[1] Currently at Université Paris-Saclay, CEA, Service d'Études Mécaniques et Thermiques, Gif-sur-Yvette, France.

https://doi.org/10.1016/j.ijrmms.2020.104582
Received 2 April 2020; Received in revised form 11 December 2020; Accepted 18 December 2020
Available online 2 June 2021

emplaced in few micro-tunnels during a pilot phase. These micro-tunnels (also called HLW disposal cells) with an excavated diameter of 0.9 m are drilled from access drifts with approximately 10 m of diameter favorably aligned with respect to the in-situ principal stress directions.[1,2] The micro-tunnels are equipped with an oil-grade ferritic-pearlitic steel casing[3] of about 0.7 m in inner diameter to prevent rock deformation and enable potential retrieval of the waste containers during the reversibility period (i.e., the possibility of reversing one or a series of steps in repository planning at any stage of the program). The casing consists in a usable part, where the HLW disposal packages are emplaced, and a head part with a diameter slightly greater than in the usable part to absorb the effects of the thrust of the usable part produced by its dilation. A cement-based grout will be used to fill the gap between the casing and the rock. A closing plug at the head part provides radiation shielding when the HLW disposal packages are not being handled. Fig. 1 shows a schematic representation of the French concept for HLW disposal cells.

The heat emitted by the HLW disposal packages causes a temperature rise within the host formation and its surrounding layers. In a water-saturated porous medium with low permeability such as the COx, the heat emitted by the exothermic waste induces a pore-pressure increase essentially due to the difference between the thermal expansion coefficient of the pore water ($\sim 10^{-4}$ 1/K) and of the solid skeleton ($\sim 1.4 \cdot 10^{-5}$ 1/K for the COx). In the planned HLW repository, the large amount of parallel, horizontal micro-tunnels will prevent the lateral displacement as well as heat and water flow between two parallel micro-tunnels. This can be explained by the repository architecture which consists in a periodic distribution of the micro-tunnels providing a symmetry effect at the mid-distance between two parallel cells in the central area of the repository. On the contrary, the whole medium can expand quasi-freely in the vertical direction.[4,5] Thermal loading thus provokes thermo-mechanical stresses in the media due to thermal expansion and mechanical confinement.

An important research program has been conducted by the French National Radioactive Waste Management Agency (Andra) to investigate the Thermo-Hydro-Mechanical (THM) behavior of the COx, through laboratory and in-situ experiments at the Meuse/Haute-Marne Underground Research Laboratory (MHM URL).[1] Several in-situ experiments were specifically designed to study the THM response of the host rock to thermal loading in small heating boreholes with diameters from 100 to 250 mm, namely the TER,[6] TED.[7] The knowledge acquired from these experiments led to a full-scale heating experiment of the 2009 French concept for HLW (no filling material is considered in the gap between the casing and the rock), called ALC experiment.[2] This in-situ experiment demonstrated the feasibility of constructing and operating a HLW disposal cell in the COx formation. The research on HLW disposal in deep geological formations has also been carried in other URLs. The FEBEX experiment based on the Spanish concept for crystalline rock was performed at the Grimsel URL (Switzerland) and provided valuable data of the near field region constituted by the compacted bentonite barrier surrounding the heater during and after its heating stage.[8] The CERBERUS, ATLAS and PRACLAY experiments are heating tests conducted at the HADES Underground Research Facility; the on-going large-scale PRACLAY aims to study the temperature effect on the near and far field behavior of the Boom clay.[9] At the Mont Terri rock laboratory in Switzerland, the HE-D and the on-going full-scale emplacement (FE) experiments take part of the experimental program for the demonstration of the Swiss concept for HLW disposal; one of their objectives is the optimization of the main components of the Engineered Barrier System that interacts with the Opalinus clay.[10] TER,[11] TED[12] and HE-D[13] experiments are some examples of small-scale in-situ heating experiments devoted to the comparison between measurements in the host rock and numerical reproduction. The modeling of these experiments performed in clayey formations have shown that the thermo-poro-elastic approach is capable to reproduce the THM behavior in the far field of the heating sources (i.e., beyond the influence of the Excavation Damaged Zone (EDZ) around the boreholes) if anisotropy is taken into account.

The main objective of this work is not only to perform a numerical modeling of an in-situ heating experiment but also to identify the possible elements to take into account when performing upscaling from a small-scale in-situ experiment to a full-scale in-situ experiment in terms of cell diameter. To the best of our knowledge, this is the first work that conducts an interpretative modeling of a small-scale in-situ heating

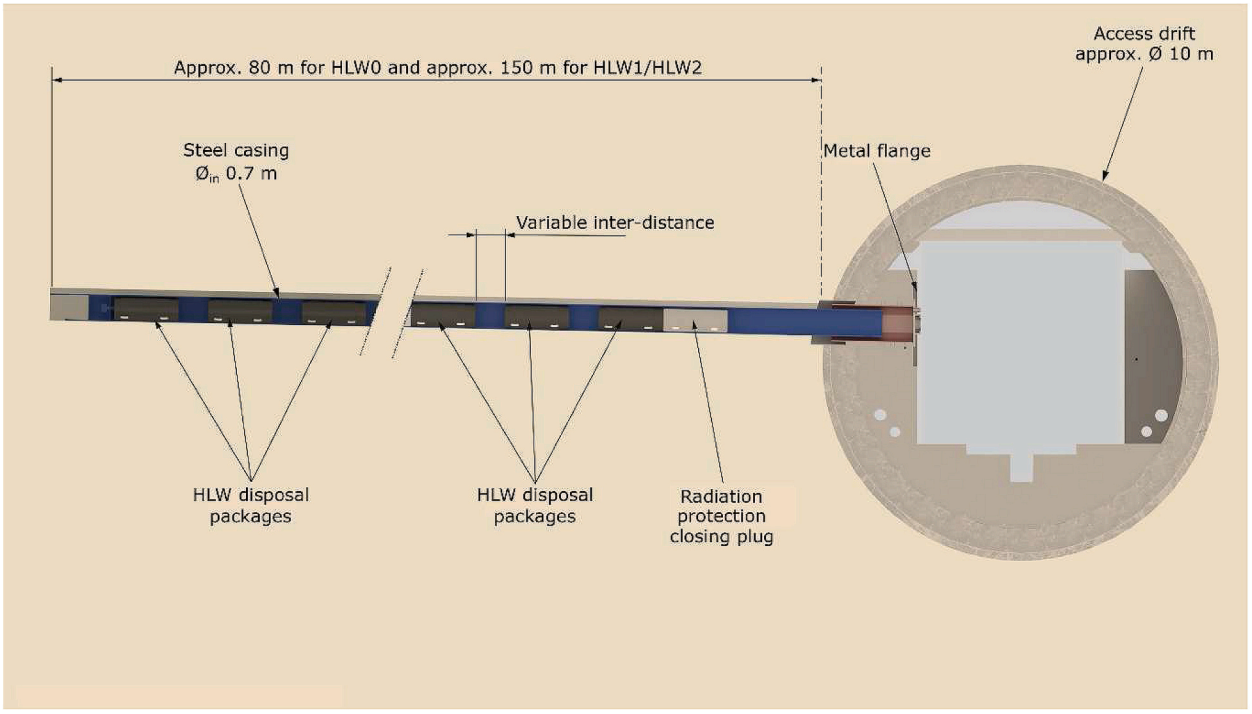

Fig. 1. Schematic representation of a HLW disposal cell (French concept).

experiment as a preliminary stage for a blind prediction of a full-scale in-situ experiment following the same approach. This is possible thanks to the collected data from two in-situ heating experiments conducted at the MHM URL: the TED (160 mm of borehole diameter) and ALC (700 mm of micro-tunnel diameter) experiments. This study has been carried out as a benchmark exercise led by Andra within Task E of DECOVALEX-2019 project (http://www.decovalex.org; https://decovalex.org/task-e.html). The upscaling modeling started with a verification test to check the numerical codes used by each team. The numerical results were compared with the analytical solution of a 3D THM coupled problem.[14,15] Then, an interpretative modeling of the TED experiment was performed to calibrate the THM parameters of the COx. The teams were provided with the pore pressure and temperature measurements at different sensor locations. Finally, the calibrated THM parameters were used for a blind prediction of the ALC experiment in the far field.

Five modeling teams participated in DECOVALEX-2019 Task E, namely; Andra, LBNL, NWMO, Quintessa, and UFZ/BGR. Table 1 shows the acronym of the teams with their respective numerical codes used in Task E. The modeling teams adopted a thermo-poro-elastic approach and assumed a transversely isotropic behavior of the COx which yielded satisfactory results in terms of temperature and pore pressure calculations, mainly in the far field.

The paper continues with a brief review of the characteristics of the COx formation in Section 2. The two in-situ heating experiments selected for the upscaling modeling are described in Section 3. A verification test of the THM formulation used by the different numerical codes is presented in Section 4. Then, the interpretative modeling of the small-scale experiment with the different modeling approaches is presented in Section 5. The numerical results of the blind prediction of the full-scale experiment using the calibrated parameters obtained for the small scale experiment are presented in Section 6. The final conclusions of this work are provided in Section 7.

2. Callovo-Oxfordian claystone

2.1. Thermo-hydro-mechanical behavior

Various small-scale investigations have been performed on the COx to determine the spatial distribution of pore size and mineral content. In Song et al.,[23] 3D reconstructions of the pore network show very low connectivity for pores larger than 40 nm which leads to a small permeability (ranging from $5{\cdot}10^{-21}$ m^2 to $5{\cdot}10^{-20}$ m^2) despite a relatively high porosity (~18%). Mineral distribution maps show a preferential orientation of carbonate and tectosilicate inclusions parallel to the bedding plane.[24] This leads to a slight anisotropy of most rock properties, particularity in terms of solute diffusion, water permeability, thermal diffusivity and mechanical parameters.

Armand et al.,[25] describes the short-term mechanical behavior of the COx as dependent on the confining pressure, as observed in other claystones. Triaxial compression tests performed on COx samples showed that the elastic limit, the peak strength, and the residual strength increase with the confining pressure. Other mechanical tests performed on samples following different orientations show a transversely isotropic behavior. The stiffness parallel to the bedding of the COx is greater than its stiffness perpendicular to the bedding (anisotropy ratio ranging between 1.2 and 2.0). Under compression loading, the strength variation in the two directions remains small and in the range of the natural variability of the COx strength. Like many other sedimentary rocks, the COx shows smaller strengths for samples oriented from 30° to 60° with respect to the bedding.

Concerning the permeability to water, a slight anisotropy ratio about 3 is observed. It is worth noting that the observed anisotropy ratio remains within the variability of the very low permeability of the COx. Horizontal thermal conductivity (i.e., parallel to the bedding) of the COx is also higher than the vertical one. Its anisotropy ratio is about 1.5.

Table 1
Modelling teams and numerical codes.

Acronym of the team	Team	Numerical code and references
Andra	French National Radioactive Waste Management Agency	COMSOL[16] and Code_Aster[17]
LBNL	Lawrence Berkeley National Laboratory	TOUGH-FLAC[18,19]
NWMO	Nuclear Waste Management Organisation	COMSOL[16]
Quintessa	Quintessa (funded by Radioactive Waste Management Limited)	COMSOL[16] QPAC[20]
UFZ/BGR	Federal Institute for Geosciences and Natural Resources and Helmholtz Centre for Environmental Research	OpenGeoSys[21,22]

2.2. In-situ stress state at the MHM URL

An anisotropic in-situ stress state is observed at the MHM URL.[26] The maximum principal stress (σ_H) is horizontal as well as the minimum principal stress (σ_h); the intermediate principal stress is vertical (σ_v). The latter two stresses have similar magnitude. At the main level of the URL (i.e., at 490 m deep) $\sigma_H \approx 16$ MPa and $\sigma_v \approx \sigma_h \approx 12$ MPa. Most of the drifts are excavated following the horizontal principal stresses at the main level of the URL. The in-situ observations show that the hydro-mechanical responses of the excavations are also affected by their orientations with respect to the in-situ stress directions.[27,28]

2.3. Theoretical formulation

The THM formulation for the modeling of the two experiments requires to take into consideration the main physical phenomena occurring when the rock is heated, treated as a fully saturated medium. The thermal load leads to hydraulic and mechanical changes within the porous medium. The pore pressure increases due to the differential thermal expansion of the pore water and the solid skeleton. Moreover, stresses develop due to both the change in temperature (thermal expansion) and the increment of pore pressure. The low permeability of the COx and its relative rigidity inhibits the dissipation of the induced pressure build-up. The mechanical effects on the hydraulic behavior are mainly limited to the near field (i.e., in the EDZ around drifts and cells). The water mobility inside the pores is so limited due to the low permeability of the COx; therefore, convection processes can be neglected and the hypothesis of a purely conductive heat transport is assumed.[29]

The general expression of the governing equations used by the modeling teams can be described for a classical thermo-poro-elastic saturated medium.[30] In recent studies, hydro-mechanical tests have shown that the Biot coefficient parallel to bedding is slightly higher than that perpendicular to the bedding.[31,32] However, this difference remains within the range of variability of the measured values and thus can be neglected. A transversally isotropic elasticity with a scalar Biot coefficient is thus considered in the formulation. In addition, the thermal expansion coefficient show little influence on the thermal pressurization coefficient[32]; therefore, the linear thermal expansion coefficient was assumed isotropic.

The momentum balance equation is described as:

$$\nabla \cdot (\boldsymbol{\sigma}' + bp\mathbf{I}) + \rho\mathbf{g} = 0 \tag{1}$$

where $\boldsymbol{\sigma}'$ is the Biot effective stress (Pa) (positive in compression), b the Biot coefficient (−), p the pore pressure (Pa), $\mathbf{I}$ the identity tensor (−), $\rho = (1-\phi)\rho_s + \phi\rho_w$ the equivalent density of the porous medium (kg/m^3) with ϕ the porosity (−), ρ_s and ρ_w the solid particle density (kg/m^3) and water density (kg/m^3), respectively, and $\mathbf{g}$ the gravity acceleration vector (m/s^2).

The Biot effective stress (Pa), $\boldsymbol{\sigma}'$ is expressed by the generalized

Hook's law as follows:

$$\boldsymbol{\sigma}' = \mathbf{C} : (\boldsymbol{\varepsilon} - \alpha_s (T - T_0)\mathbf{I}) \tag{2}$$

where $\boldsymbol{C}$ is the 4th order elasticity tensor (Pa) and $\boldsymbol{\varepsilon}$ is the strain tensor (−), α_s is the linear thermal expansion coefficient of the solid skeleton (1/K), T is the temperature (°C) and T_0 is the reference temperature (°C).

The water mass balance equation that describes the hydraulic process is given by:

$$\frac{d(\phi\rho_w)}{dt} + \phi\rho_w \frac{\partial \varepsilon_v}{\partial t} + \nabla \cdot (\rho_w \mathbf{v}) = 0 \tag{3}$$

where ε_v is the volumetric strain (−) and $\mathbf{v}$ is the seepage velocity (m/s) defined by the generalized Darcy's law:

$$\mathbf{v} = -\frac{\mathbf{K}}{\mu}(\nabla p - \rho_w \mathbf{g}) \tag{4}$$

where $\boldsymbol{K}$ is the intrinsic permeability tensor (m^2) and μ is the fluid dynamic viscosity (Pa·s).

The thermal process is described by the heat transport equation in the following form:

$$(\rho C)_{eff} \frac{dT}{dt} - \nabla \cdot (\boldsymbol{\lambda} \nabla T) + \rho_w C_{p,w} \mathbf{v} \cdot \nabla T = Q \tag{5}$$

where $(\rho C)_{eff} = (1-\phi)\rho_s C_{p,s} + \phi\rho_w C_{p,w}$ is the effective heat capacity (J/m^3/K) with $C_{p,w}$ the specific heat capacity of water (J/kg/K), $C_{p,s}$ the specific heat capacity of solid skeleton (J/kg/K), λ is the effective thermal conductivity tensor of the porous medium (W/m/K), and Q is the heat source (W).

Water properties are expressed differently by the modeling teams. This proved to be a distinctive factor when comparing the numerical results in the different steps. UFZ/BGR used the IAPWS equations for water density and water dynamic viscosity (IAPWS R7-97 and IAPWS 2008, respectively), which consider their non-linear behavior under temperature and pressure variations. LBNL used the IFC-1967 formulation for the water properties. Quintessa chose the Rowe-Chou[33] and Sharqawy[34] equations for water density and dynamic viscosity, respectively. Andra and NWMO expressed the density as follows[35]:

$$\rho_w = \rho_{w0} \exp[C_w(p - p_0) - \alpha_w(T - T_0)] \tag{6}$$

where ρ_{w0} is the reference density (kg/m^3), C_w is the water compressibility (1/Pa), p_0 is the reference pressure (Pa). The volumetric thermal expansion coefficient is a function of temperature and the relationship was linear for Andra and nonlinear for NWMO giving slightly higher values for the latter as shown in Fig. 2.

The dynamic viscosity expression used by Andra and NWMO depends on the temperature[36]:

$$\mu = A \exp(B / T) \tag{7}$$

with $A = 2.1 \cdot 10^{-6}$ Pa s and $B = 1808.5$ K.

3. Description of the in-situ heating experiments

3.1. TED experiment

The TED experiment aimed to reproduce the THM response of the COx due to the interaction between parallel heating sources in a configuration similar to the French concept for HLW, but at a small-scale.[7] This experiment enabled development of numerical models to predict the THM behavior of the undisturbed rock mass in the far field (i.e., beyond the influence of the EDZ). The heating phase started on 25th January 2010 (divided into two stages) and ended on 22nd October 2012, followed by a cooling phase lasting nine months.

The experiment was located in the GED drift and consisted of three

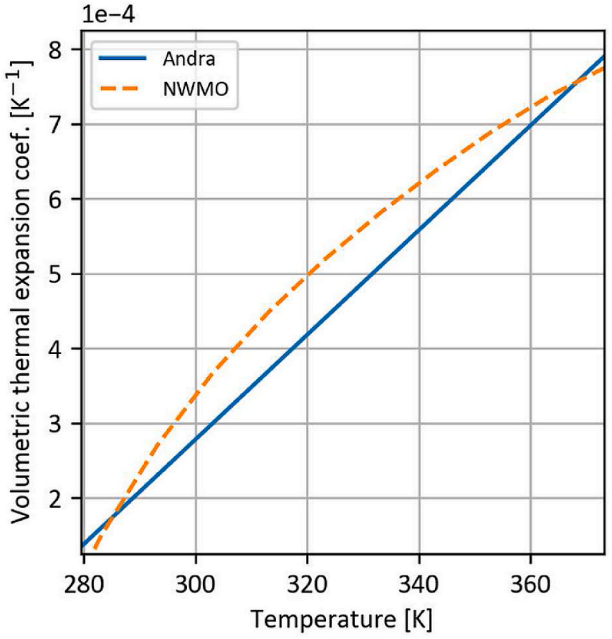

Fig. 2. Considered variation of the volumetric thermal expansion coefficient of water with temperature used by Andra and NWMO.

4 m long heating devices which were installed at the end of 160 mm diameter and 16 m long boreholes (TED1201, TED1202, and TED1203) in order to avoid the influence of the temperature variations of the GED drift. These three boreholes were drilled parallel to the maximum horizontal stress with a spacing of about 2.7 m.

The experiment was heavily instrumented with more than 200 sensors recording temperature and pressure in the host rock (Fig. 3). They were installed in twenty three boreholes: twelve boreholes for measuring pore pressure (TED1250 to TED1259, TED1240, and TED1241), nine boreholes for temperature measurements (TED1210, TED1212 to TED1219), and two boreholes for displacement measurements (TED1230 and TED1231). Their locations were selected to evaluate the anisotropic THM response of the host rock. Most of the sensors were located at 14 m distance from the GED drift (i.e., mid-section of the heaters).

The heater boreholes, TED1230, and TED1231 were not backfilled but grouted by metal tubing and surrounded by a cement layer. As a consequence, drainage of water through these boreholes influenced the local pressure field.

Fifty-one sensors were installed in the external casing of the heater boreholes to monitor its temperature and eighteen sensors inside the heaters to monitor and regulate the temperature. Finally, temperature sensors were installed for the air temperature in the GED drift (TED1270 to TED1277).

The excavation of the GED drift started on 21st April 2008 and ended on 22nd January 2009. The passage at the level of the TED area was on 6th September 2008. The installation of the instrumentation started on 1st July 2009 and finished with the installation of the heaters on 6th November 2009.

The nominal power to be applied in each heater was designed to reach a maximum temperature of 90 °C at the rock-heater interface when the three heaters were switched on. This maximum value was based on the thermal criterion for the designing of the HLW repository: the maximum temperature in the COx formation have to be lower than 90 °C.

The power history included three main stages. Only the central heater was switched on during the first stage, which started at a relatively low heating power of 150 W on 25th January 2010, followed by two steps at 300 W and finally 600 W (each of the three steps being

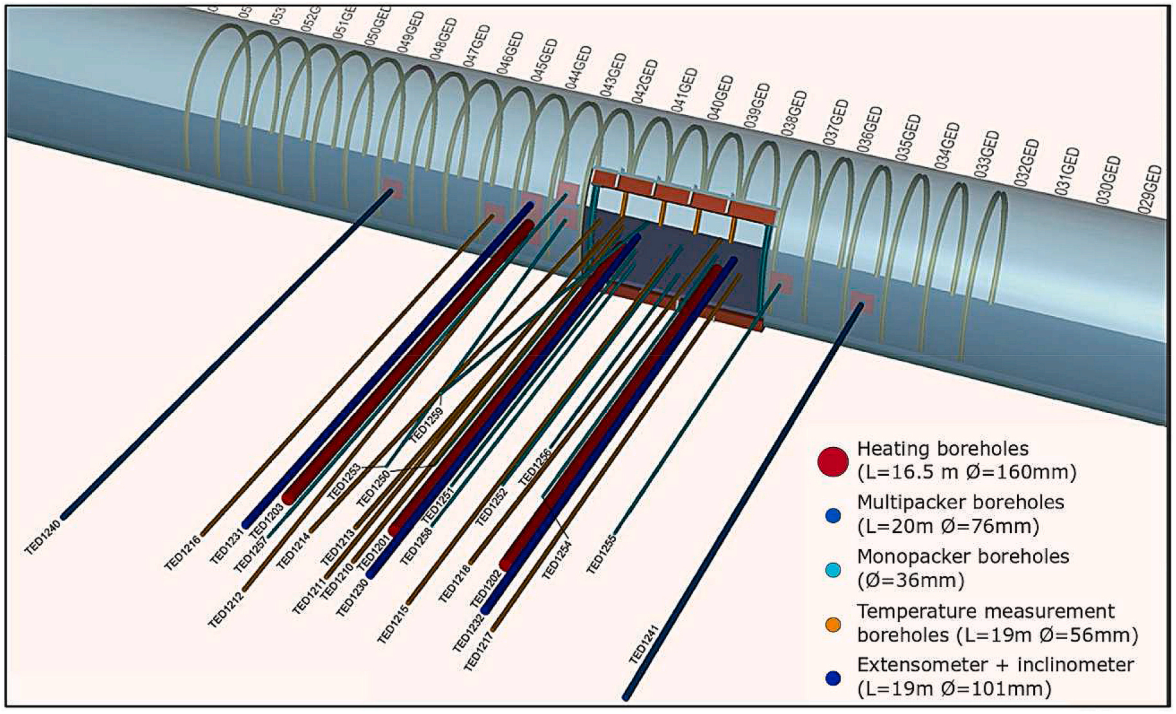

Fig. 3. Three-dimensional layout of the TED experiment (From Conil et al.[7]).

about four months long). One year later, the two surrounding heaters were turned on in the same power steps used for the first heater from 1st March 2011 until 22nd October 2012. In a last cooling stage, the power was decreased by 50 W every month until the final shutdown on 19th July 2013 (Fig. 4).

During the different stages, the input power was maintained long enough to achieve a quasi-steady state. Some significant cut-offs (heater outages) occurred during the experiment but most of them lasted only a few hours and did not impact the pressure and temperature measurements in the rock mass. However, a 48-h-long cut-off led to large pressure and temperature drops in the closest boreholes.

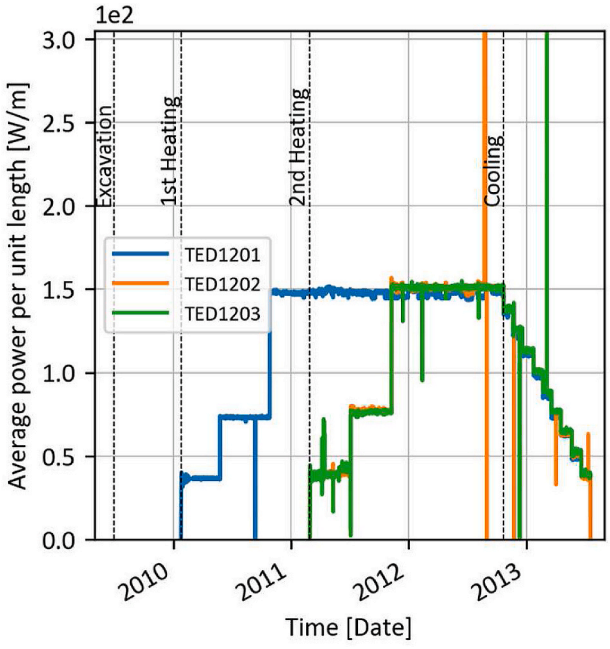

Fig. 4. Timeline of the TED experiment with the evolution of the heat power applied during its different stages (Adapted from Conil et al.[7]).

3.2. ALC experiment

The ALC experiment is a full-scale demonstrator of the 2009 French concept for one single HLW disposal cell (no filling material is considered in the gap between the casing and the rock). The main objectives were to Ref.[2]: (1) test the feasibility of such disposal, (2) study the thermo-mechanical behavior of the cell and its interface with the host rock, and (3) study the THM behavior of the host rock as previously done in TER and TED experiments. Unlike the TED experiment, the ALC experiment was at its heating stage at the time of this work, thus no cooling phase was considered.

The experiment consists of a micro-tunnel (ALC1604), drilled from the GAN drift parallel to the maximum horizontal stress; it has a total length of 25 m. The ALC1604 micro-tunnel is divided into two parts: a head part of 6 m long with an excavated diameter of 0.791 m and a usable part of 19 m long with an excavated diameter of 0.75 m. The head part has a steel insert, with 0.767 m external diameter and 21 mm thick, and the usable part has a casing, with 0.70 m external diameter and 20 mm thick. There is an overlap zone of 1 m width between the casing and the insert (i.e., between 5 and 6 m from the GAN drift wall). The heated part is located in the usable part between 10 and 25 m deep and is made up of five 3 m long heating devices. An overview of the ALC1604 micro-tunnel and the instrumentation boreholes is shown in Fig. 5.

A schematic representation of the ALC1604 micro-tunnel (cross-section) including the steel casing, the heater and the theoretical initial average value of the annular space at vault and sides (i.e., the gap between the casing and the rock) is given in Fig. 6. The annular space changes over time due to the convergence of the cell wall, which includes distortion of the casing into an oval shape. The COx is in full contact with the casing 400 days after the micro-tunnel excavation.[2]

Nine peripheral boreholes were drilled both from the GAN drift and the NRD niche, which is itself excavated from the GRD drift: six boreholes for pore pressure and temperature measurements (ALC4001, ALC4002, ALC4005, and ALC1616 to ALC1618), two boreholes for temperature measurements (ALC4003 and ALC1633) and one borehole

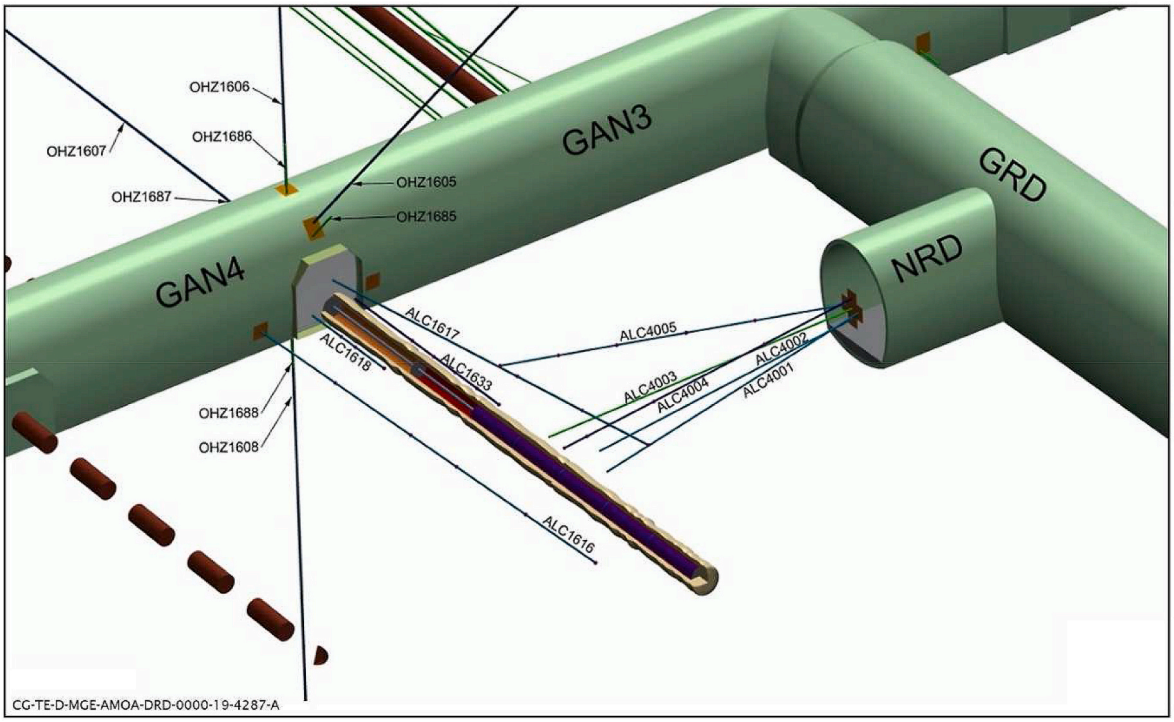

Fig. 5. Three-dimensional layout of the ALC experiment (From Bumbieler et al.[2]).

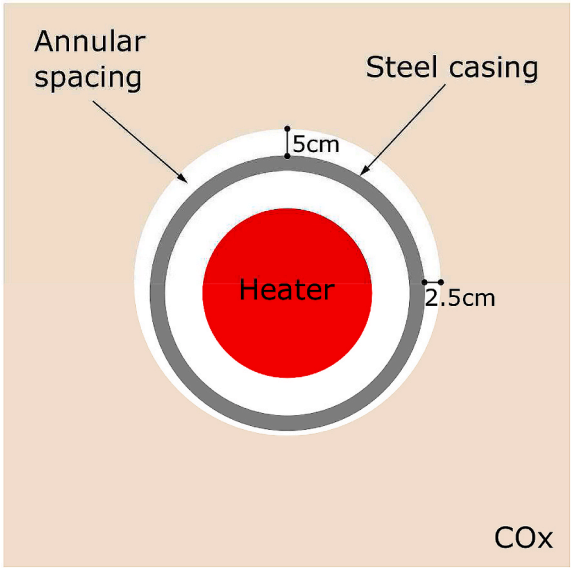

Fig. 6. Schematic representation of the ALC1604 micro-tunnel at its initial state.

(ALC4004) equipped with twenty extensometers.

The casing and the insert were instrumented to study the thermo-mechanical behavior of the cell and the contact with the rock. The air temperature and convergence of the GAN drift were also monitored (OHZ1605 to 1608, OHZ1685 to 1688).

The GAN drift was excavated in several phases from 3rd November 2009 to 6th February 2012. The drift-face passed by the ALC1604 location on 3rd May 2011. The first 27 m of the GRD drift close to the GAN drift were excavated from 16th December 2010 to 7th April 2011.

Almost all the peripheral boreholes (OHZ1605 to 1608, OHZ1685 to 1688, ALC4001 to ALC4005, ALC1616 and ALC1617) were drilled and installed between 17th October 2011 and 17th November 2011. The last two peripheral boreholes (ALC1618 and ALC1633) were drilled and installed between 12th November 2012 and 14th November 2012. The ALC1604 micro-tunnel was excavated and cased between 23rd October 2012 and 26th October 2012.

A heating test at low power (33 W/m) was first conducted between 31st January and 15th February 2013. The main heating phase started on 18th April 2013, at a constant nominal power of 220 W/m. A few significant breakdowns occurred during the experiment on one single heating element at a time. These breakdowns did not disrupt the global temperature in the casing given that the other four heater elements continued to work.

4. Verification of the numerical codes (step 1)

The numerical models were verified against an analytical solution of a 3D thermo-hydro-mechanical problem in order to limit the comparison bias. Booker and Savvidou[14] provided an analytical solution of an infinite homogeneous saturated elastic porous medium around a constant point heat source, Q [W]; the pore water and the solid grains are assumed incompressible. Therefore, the verification test considers a Biot coefficient equals to 1.0 despite the fact that the experimental values obtained for COx vary between 0.6-1.0. The analytical solution for the stress tensor has been corrected recently in Ref.[15]

The modeling teams were requested to represent the domain (an eighth of the total geometry) with a cube of 15 m x 15 m x 15 m. The heat source Q was modeled either by a point or a small cylinder centered at the coordinates (0, 0, 0), oriented along the axis z, of a 1 mm radius and 1 mm height. The initial conditions of the medium consider a null stress state, 0 MPa, as well as the temperature and the pore pressure, 0 °C and 0 MPa, respectively.

Regarding the boundary conditions, the three symmetry planes are impermeable, adiabatic and free to move in the two directions parallel to their respective planes. The far field boundaries correspond to their initial conditions (Table 2). At the heat source, a constant heat power of $Q = 700$ W is instantaneously applied at time $t = 0$ days, taking into account the 1/8th symmetry of the domain being modeled. The THM parameters of the porous medium are listed in Table 3. The hydro-

Table 2
Boundary conditions for the verification test.

Boundary	Mechanical	Hydraulic	Thermal
Symmetry boundaries	Zero normal displacements	Zero fluid flow	Zero Heat flux
External boundaries	Free surface	0.0 MPa	0.0 °C

Table 3
THM parameters for the verification test.

Parameter	Unit	Symbol	Values
Young's modulus	Pa	E_y	$4.5{\cdot}10^{9}$
Poisson's ratio		ν	0.3
Porosity		ϕ	0.15
Equivalent thermal conductivity	W/m/K	λ	1.7
Equivalent density	kg/m^3	ρ	2400
Equivalent heat capacity	J/kg/K	$C_{p,eq}$	1000
Density of solid grains	kg/m^3	ρ_s	2700
Heat capacity of solid grains	J/kg/K	C_{ps}	773
Intrinsic permeability	m^2	K	$4.5{\cdot}10^{-20}$
Volumetric coefficient of thermal expansion of solid grains	1/K	α_s	$4.2{\cdot}10^{-5}$
Density of water	kg/m^3	ρ_w	1000
Compressibility of water	1/Pa	C_w	0.0
Heat capacity of water	J/kg/K	$C_{p,w}$	4180
Dynamic viscosity of water	Pa·s	μ_w	$1.0{\cdot}10^{-3}$
Volumetric coefficient of thermal expansion of water	1/K	α_w	$4.0{\cdot}10^{-4}$

mechanical parameters are based on[27] and the thermal parameters on.[7]

The numerical results of the temperature, the pore pressure, the displacement field and the stresses were compared against the analytical solution at four points near the heating source. In this paper, only the results for the temperature and pore pressure at point P1 whose coordinates are (x, y, z) = (0.35, 0.0, 0.0) are presented.

All teams obtained good agreement between the numerical results and the analytical solution despite the use of different codes and the slight differences in the formulation or the representation of the point heat source.

Fig. 7 shows the results of the evolution of the temperature and the pore pressure at point P1 obtained by all five teams along with the analytical solution. The calculated temperatures match the analytical solution with slight differences as well as the pore pressure.

Fig. 8 shows the evolution of the pore pressure at point P1 to study how the numerical results differ from the analytical solution, if we consider only (A) water compressibility or (B) non-constant water properties (i.e., the dynamic viscosity and the thermal expansion coefficients vary with the temperature and pore pressure). These additional simulations have been performed to explore the influence of these variations on the obtained results. It is worth reminding that the analytical solution[14] is valid only for constant material properties. The numerical results show that ignoring the water compressibility overestimates the pore pressure. NWMO used a compressibility coefficient equal to $4.0{\cdot}10^{-10}$ 1/Pa, whereas Andra and Quintessa used a value of $5.0{\cdot}10^{-10}$ 1/Pa. The pore pressure is also significantly lower than the one obtained by the analytical solution when considering non-constant water properties and the pore pressure build-up is delayed mainly due to the variation of the thermal expansion coefficient with temperature (the constant value used for the analytical solution is $4.0{\cdot}10^{-4}$ 1/K, which approximately correspond to 42 °C, considering the relationships in Fig. 2).

The five numerical codes used by the five teams successfully reproduced the analytical solution of the THM behavior of a saturated porous medium subjected to a heat source. The temperature- and pressure-dependence of the water properties play an important role in the prediction of the pore pressure and eventually on the mechanical prediction of the model. Thus, these features should not be ignored when modeling realistic situations. In addition, the use of different equations for the description of the water properties may lead to slightly different numerical results between the modeling teams.

5. Calibration of the TED experiment (step 2)

5.1. Model set-up

The modeling specifications for the numerical 3D representation of the TED experiment included the GED drift with 4.6 m diameter and the heater boreholes (TED1201, TED1202, and TED1203) with 0.16 m diameter. In addition, the extensometer boreholes TED1230 and TED1231 with 0.076 m diameter were also included in the geometry

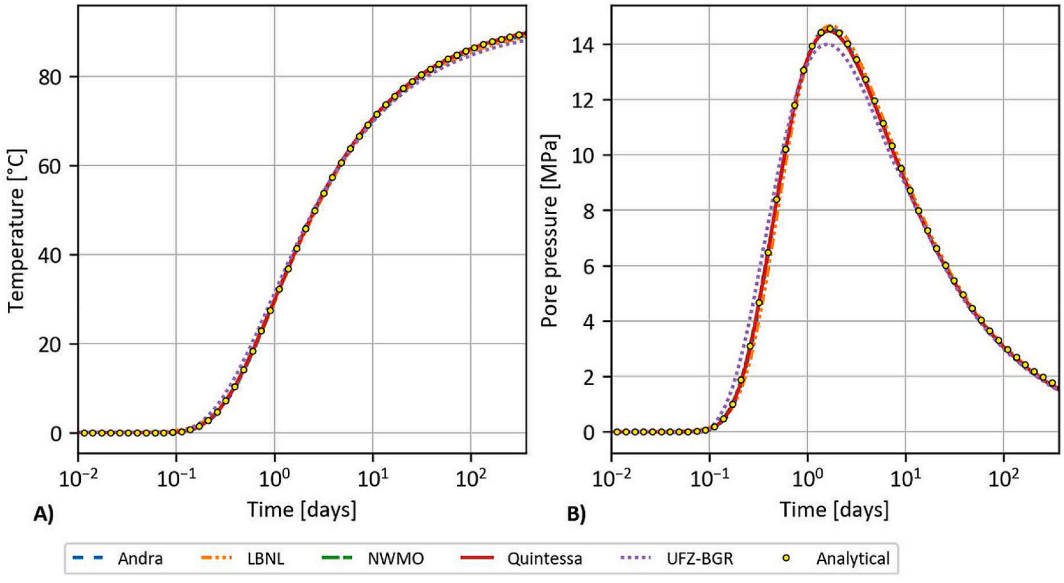

Fig. 7. Numerical results of the verification test at point P1: (A) temperature and (B) pore pressure.

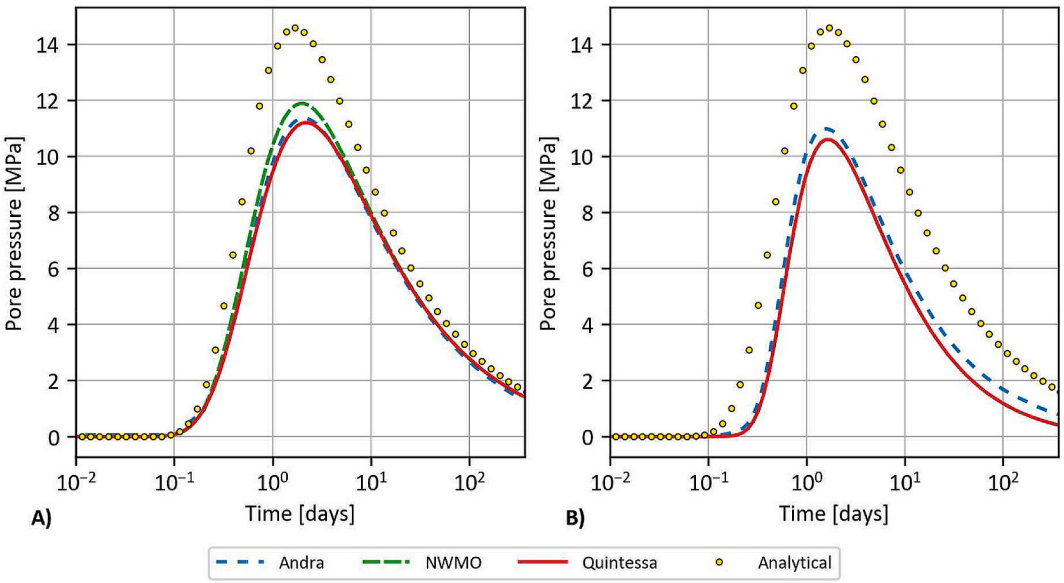

Fig. 8. Pore pressure evolution of the verification test at point P1 assuming (A) water compressibility and (B) water properties depending on temperature and pressure.

since they showed to be draining and to locally affect the pore pressure. Other boreholes that are considered watertight were not explicitly represented in the models.

The considered geometry consists of a cube with a side length of 50 m (a distance set to represent the far field) centered in height at z = 0. Only half of the GED drift is represented, in a way that one face of the cube coincides with the cross-section plane at y = −2.3 m. The cube coordinates vary between x = −25 m to +25 m, y = −2.3 m to +47.7 m, and z = −25 m to +25 m.

The teams were asked to concentrate on the heating phase and not to spend too much time on the GED drift excavation and borehole drilling modeling since a complete determination of the initial state would need a whole study employing sophisticated models. Therefore, the determination of an accurate initial pore pressure and stress state was not necessarily essential. It was assumed that the pressure and stress field are not so much affected by the presence of the EDZ around GED; the fractured zone around the GED drift represents an important vertical extent (up to 1 diameter) and a limited horizontal extent due to its orientation with respect to the stress state.[28] The results of hydraulic conductivity measurements near the GED drift, shown in Fig. 9, were considered for the modeling of the EDZ around the GED drift.

With these elements in mind, the simulation starts with an initialization step before the excavation of the GED drift. The initial stress state is: a) the maximum principal total stress, σ_H = 16.1 MPa, equals to the total stress in the y direction, σ_y, b) the minimum principal total stress, σ_h = 12.4 MPa, equals to the total stress in the x direction, σ_x, and c) the intermediate principal total stress, σ_v = 12.7 MPa, equals to the total stress in the z direction, σ_z. The initial pore pressure is uniform and equals to 4.7 MPa. The temperature field respects the geothermal gradient of 0.04 K/m with a temperature of 22.0 °C at 490 m deep (z = 0 m). The numerical results are presented from the date of the borehole drilling (i.e., 1st July 2009).

Atmospheric pressure and thermal conditions determined from the temperature measurements are applied on the GED drift wall (the

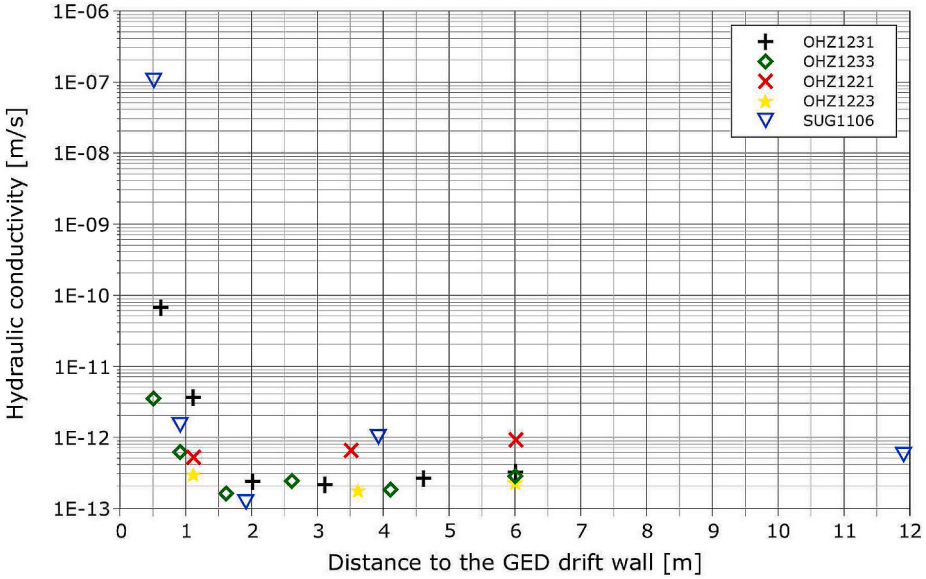

Fig. 9. Horizontal hydraulic conductivity measured during several tests near the GED drift (Adapted from Armand et al.[28]).

temperature evolution can be found in Ref.[7] A mechanical pressure equals to 0.3 MPa is also applied to represent the shotcrete lining.

The teams were free to use intermediate or fully draining conditions on the borehole walls when the water tightness cannot be guaranteed. It was recommended to constraint the normal displacements. No heat flux was imposed prior to the heating phase. The heaters were emitting less heat than the designed heater output according to the observed temperature measurements. Therefore, the heating phase was modeled with 95% of the total heating power emitted from the boreholes.

The teams were asked to calibrate their models against experimental data by adjusting the different THM parameters from reference values or reference range of values, depending on the uncertainty about the parameters. These reference values and reference range of values are summarized in Table 4. The hydraulic parameters are based on,[27,31,32] and the thermal parameters on.[7]

No mechanical parameters were given since the teams were free to use different mechanical models to reproduce the COx behavior. Thus, results of a set of laboratory tests performed on COx samples[25] were meant to be calibrated by each team to determine the mechanical parameters of their models.

The thermal parameters were calibrated by comparing the measurement data at six selected points with the numerical solutions. In this work, the numerical results at two sensors are presented (TED1210_05, TED1219_05). The hydraulic properties were calibrated by comparing the numerical results with the measurements acquired at one pair of pressure sensors, one sensor perpendicular and another one parallel to the bedding plane, in the mono-packer boreholes TED1253_01 and TED1258_01. The coordinates of these measurement points are listed in Table 5; all these points are located on the mid-section plane of the heaters (y = 14.0 m).

The study of the pore pressure gradient towards the drift wall was based on the pressure measured in a multi-packer borehole at far field from the experiment, the TED1240 borehole, which contains five sensors (Table 5).

5.2. Modeling approaches

All teams calibrated the thermal parameters by carrying out a thermal analysis of the heating phase. The influence of the hydraulic and mechanical response on the thermal response was considered negligible since the dominant heat transfer mechanism is conduction.

Hydraulic parameters were obtained by running coupled THM, HM and/or TH simulations of the GED drift excavation and the heating phase. The main goal of these preliminary simulations was to calibrate appropriate values of the Young's modulus and permeability perpendicular and parallel to the bedding plane. All teams assumed an elastic homogeneous anisotropic behavior for the COx. Therefore, the THM coupling is based on the thermo-poro-elasticity theory following the same approach used in the verification test. Each team calibrated their model in a different way to reproduce the observations in the experiment, in particular the teams used different parameterization of the hydraulic process; some teams partially modified the boundary conditions provided in the task specifications. The differences in the models led to variations of temperature and pore pressure between the teams.

The changes of the water properties such as density, fluid dynamic viscosity and thermal expansion coefficient with temperature and pore pressure were taken into account by all teams as discussed in section 4.

The increased EDZ permeability around the GED drift was either modeled by an EDZ of 1 m thick with a constant increased permeability (Andra, LBNL and Quintessa) or by taking into account the permeability enhancement over the first meters from the GED drift wall (NWMO and UFZ/BGR) as shown in Fig. 9. Further details of the two latter approaches can be found in Ref.[37] and[38] respectively.

Regarding the initial and boundary conditions, the GED drift excavation as well as borehole drilling were simulated instantaneously by the modeling teams. Andra and LBNL chose to impose intermediate drained conditions on the borehole walls by modeling a porous medium with higher permeability than the COx ($\sim 10^{-15}$ m^2) after the drilling phase. Quintessa and NWMO used fully drained conditions on the borehole walls. Unlike the other teams, UFZ/BGR uses three lines for modeling of the heater boreholes (power source along a polyline) as well as the extensometers boreholes, all of them with fully draining boundary conditions.

LBNL solved the thermo-poro-elastic model by using a sequential coupling scheme described in Ref.[39] that links TOUGH2 with FLAC3D, a multiphase fluid flow and heat transport simulator, and geomechanical code, respectively. The other teams undertook fully coupled simulations.

In addition to the full THM representation, Quintessa used a TH formulation that assumes coupling with the mechanical process only by defining the porosity as a function of pressure and temperature. In this way, the computational time decreases significantly without affecting the thermo-hydraulic response.[40] The model used with this formulation did not represent the initial conditions caused by the excavation tunnel and only pressure increments were analyzed, which was useful for the calibration stage. The presented results for Quintessa are for the full THM model; results for the TH model can be found in Ref.[40]

Table 4
Reference THM values for parameter calibration.

Parameter	Unit	Symbol	Values
Porosity		ϕ	0.15–0.18
Thermal conductivity parallel to bedding	W/m/K	λ_h	1.96
Thermal conductivity perpendicular to bedding	W/m/K	λ_v	1.26
Equivalent density	kg/m^3	ρ	2400
Equivalent heat capacity	J/kg/K	$C_{p,eq}$	1000
Density of solid grains	kg/m^3	ρ_s	2600
Heat capacity of solid grains	J/kg/K	C_{ps}	800
Intrinsic permeability parallel to bedding	m^2	K_h	$6.0{\cdot}10^{-21}$ - $6.0{\cdot}10^{-20}$
Intrinsic permeability perpendicular to bedding	m^2	K_v	$3.0{\cdot}10^{-21}$ - $3.0{\cdot}10^{-20}$
Biot coefficient	–	b	0.6–0.85
Volumetric thermal expansion of solid grains	1/K	α_s	$4.2{\cdot}10^{-5}$

Table 5
Measurement points for parameter calibration.

Sensor	Direction to the bedding plane	Coordinates (x, y, z)	Type of measure
TED1210_05	Perpendicular	(-0.06, 14.01, 0.61)	Temperature
TED1219_05	Parallel	(-0.59, 13.96, −0.09)	Temperature
TED1253_01	Parallel	(1.10, 14.08, −0.13)	Temperature and pressure
TED1258_01	Perpendicular	(0.20, 14.13, −1.34)	Temperature and pressure
TED1240_01	Parallel	(7.01, 19.92, −0.15)	Pressure
TED1240_02		(6.91, 13.90, −0.08)	Pressure
TED1240_03		(6.85, 10.39, −0.04)	Pressure
TED1240_04		(6.80, 7.89, −0.01)	Pressure
TED1240_05		(6.75, 4.88, 0.02)	Pressure

5.3. Results

The temperature measurements show that the rock exhibits a transversely isotropic thermal response. The temperature increases at a given distance from the heater are higher parallel to the bedding plane than in the perpendicular direction. All teams obtained similar results for temperature predictions and were able to capture the transverse isotropy of the thermal response (Fig. 10). The measurements are represented by yellow circles and the numerical results by lines. These results are in accordance with the low dispersion of the calibrated thermal parameters (Table 6). In addition, the thermal conductivity coefficients in both directions fall into the range of values obtained in laboratory tests on COx samples given in Ref.[1] except for $\lambda_h = 2.26$ which is slightly higher.

The calibrated hydro-mechanical parameters (Table 7) show a higher dispersion than the thermal parameters, particularly, the permeability values and their corresponding degree of anisotropy. This may be a consequence of the different approaches followed by the teams in addition to the uncertainty of the intrinsic permeability.

Observations of pore pressure also show the anisotropic response due to the anisotropic properties of the COx. Fig. 11 show the pore pressure evolution at two sensors located perpendicular and parallel to the bedding, respectively. The measurements are represented by yellow circles and the numerical results by lines. The numerical results show that the anisotropy was well captured by the teams. There is a lower level of agreement between the teams in the pressure results than the thermal results. This is likely due to the pressure response being a coupled response, depending on more processes and parameters in the models than the thermal response. The teams experienced difficulties in achieving a correct reproduction of the pore pressure due to the excavation of the GED drift, but this was not the main focus of the task.

The pore pressure build-up is consistent with the heating stages and the dispersion of the results is more limited in the horizontal direction (TED1253_01). However, the pressure peaks are either globally underestimated (TED1258_01) or overestimated (TED1253_01).

Fig. 12 show the pore pressure evolution at two sensors located relatively far from the heating boreholes. The numerical comparison against the measurement data shows that all teams underestimate the pressure change due to heating at sensor TED1240_02. This may be due to the spatial variability in the COx properties and representing the temperature evolution at these measuring points would help to understand these differences. Unfortunately, temperature measurements were not provided for these points.

Table 6
Calibrated thermal parameters.

	λ_h	λ_v	C_p
	W/m/K	W/m/K	J/kg/K
Andra	1.97	1.29	1000
LBNL	2.05	1.15	1000
NWMO	2.01	1.28	1000
Quintessa	2.01	1.30	1000
UFZ-BGR	2.26	1.40	1000

The numerical results of the interpretative modeling of the TED experiment has shown that the thermal models work correctly and consistently for all the teams (e.g., absolute values are well reproduced, the anisotropy of the temperature evolution is captured). According to the observed temperature measurements, the heaters emit less heat than the designed heater output. Therefore, all the modeling teams agreed to use a correction coefficient of 95% to account for the power loss within the heaters which were then used for the ALC experiment.

The modeling of the drillings of the boreholes with the poro-elastic models were quite consistent with the pore pressure values measured parallel to the bedding, whereas the pressure perpendicular to the bedding was not well reproduced; this did not have a significant impact during the heating. The general trend of the pressure build-up due to the temperature increase is well reproduced. The anisotropy of the pressure response is also captured. According to the results, the two major factors in the pore pressure description are the permeability, the Young's modulus, and their anisotropy ratios. The permeability values that best reproduced the local and global maxima pore pressure were around $3{\cdot}10^{-20}$ m^2 and 10^{-20} m^2 in the direction parallel and perpendicular to the bedding, respectively.

6. Blind prediction of the ALC experiment (step 3)

6.1. Model set-up

It was specified that the geometry models should include the GAN drift, the GRD drift and the ALC1604 micro-tunnel. Moreover, the models may explicitly represent the extensometer borehole (ALC4004)

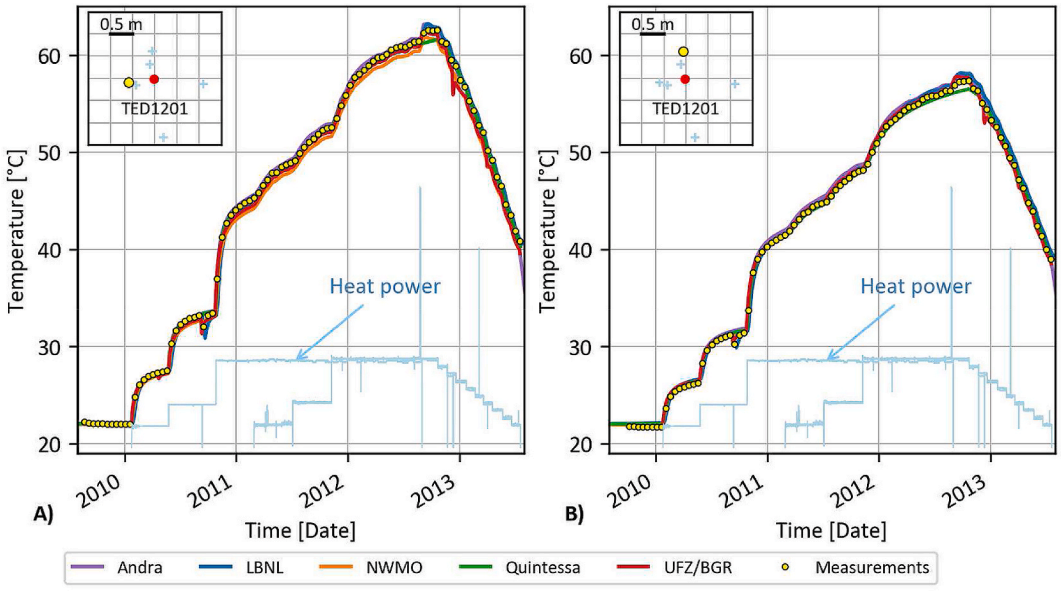

Fig. 10. Temperature evolution at sensors: (A) TED1219_05, located parallel to bedding and B) TED1210_05, located perpendicular to bedding. The heat power history is plotted in light blue. (For interpretation of the references to colour in this figure legend, the reader is referred to the Web version of this article.)

Table 7
Calibrated hydro-mechanical parameters.

	E_{yh}	E_{yv}	ν_{hv}	ν_{Hh}	b	ϕ	K_h	K_v
	10^9 Pa	10^9 Pa	–	–	–	–	10^{-20} m^2	10^{-20} m^2
Andra	8.0	5.0	0.3	0.3	0.6	0.15	2.5	0.6
LBNL	6.0	3.0	0.3	0.3	0.7	0.15	3.0	0.7
NWMO	5.8	3.4	0.25	0.3	0.6	0.15	2.9	0.8
Quintessa	6.0	3.0	0.3	0.3	0.6	0.15	5.0	1.0
UFZ/BGR	6.0	1.53	0.33	0.33	0.6	0.15	2.9	0.8

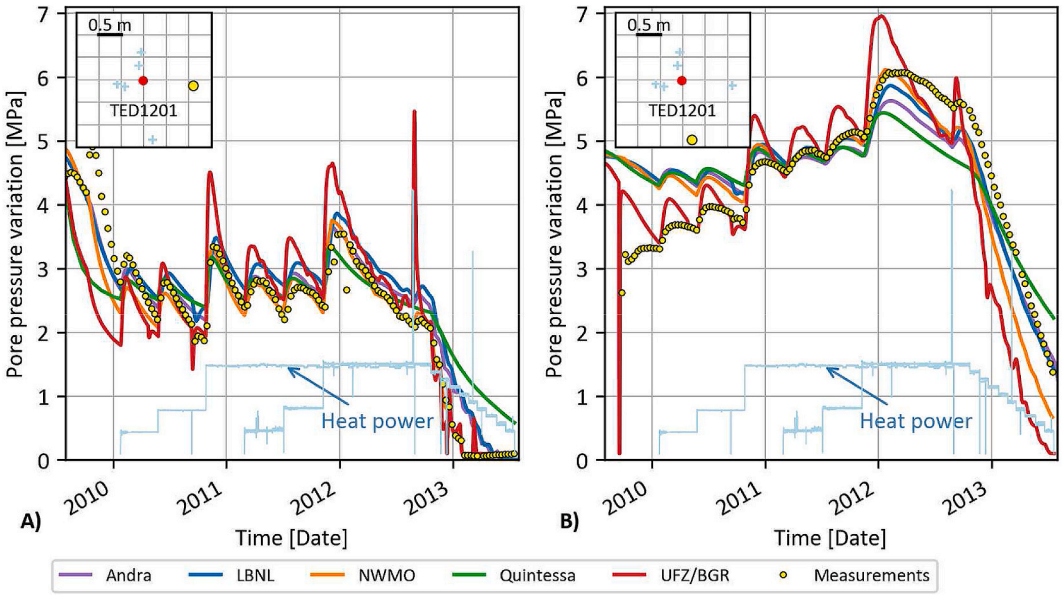

Fig. 11. Pressure evolution at sensors: (A) TED1253_01, located parallel to bedding, (B) TED1258_01, located perpendicular to bedding. The heat power history is plotted in light blue. (For interpretation of the references to colour in this figure legend, the reader is referred to the Web version of this article.)

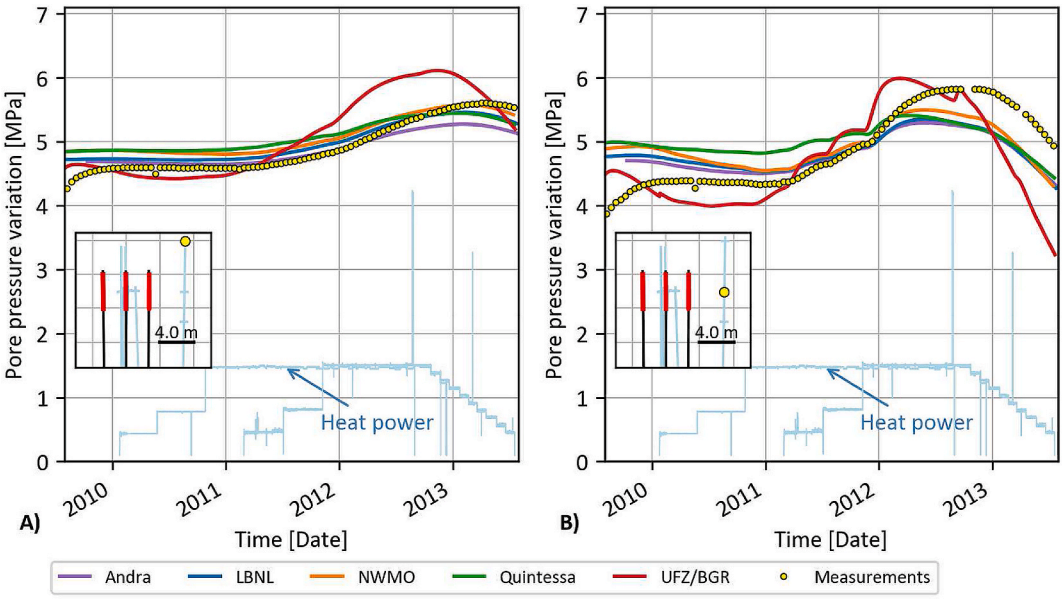

Fig. 12. Pressure evolution at sensors: (A) TED1240_01 and (B) TED1240_02. The heat power history is plotted in light blue. (For interpretation of the references to colour in this figure legend, the reader is referred to the Web version of this article.)

that could be draining and locally affecting the pore pressure field.

The models used the local axis system that was defined for the ALC experiment; its origin (0,0,0) is the head of the ALC1604 micro-tunnel. The x-axis coincides with the cell axis and the y-axis coincides with the GAN drift axis. The domain consisted of a cube with a side length of 50 m; this geometry corresponds to the distance between the cell and the

GRD drift and is considered large enough regarding the diameter of the ALC cell. The cube is centered at height z = 0. The models represented only half of the GAN drift (radius = 2.6 m) and half of the GRD drift (radius = 2.85 m), in a way that one face of the cube coincides with the cross-section plane at x = −2.6 m and another face coincides with the cross-section plane at y = 21.6 m. Thus, the cube coordinates vary between x = −2.6 m–47.4 m, y = −28.4 m to 21.6 m, and z = −25 m–25 m.

The initial conditions were obtained in the same fashion as for the TED experiment, with the exception of the principal stress orientation. For the configuration of the ALC experiment, the maximum principal total stress, σ_H, coincides with σ_x (i.e., parallel to the cell axis), the minimum principal total stress, σ_h, is parallel to the y-axis, and the intermediate principal total stress, σ_v remains oriented in the z direction. The thermal field respects the geothermal gradient of 0.04 °C/m with a temperature of 22.0 °C at 490 m deep (z = 0.0 m). The drifts' excavation affects the hydro-mechanical initial state. For the modeling purposes, it was assumed that the initial pore pressure field around the ALC cell is mainly controlled by the excavation and presence of the GAN and the GRD drifts. It was assumed that the pressure and the stress fields were not so much affected by the presence of the damaged zone around GAN given that the heating part of the cell is located far from the drift wall (10–25 m). The simulations were required to set the initial time on 23rd October 2012, corresponding to the beginning of the cell excavation.

The boundary conditions follow the same specifications as for the modeling of the TED experiment. The temperature evolution on the gallery walls are given in Fig. 13; atmospheric pressure and a mechanical pressure of 0.3 MPa are applied on the gallery walls.

All instrumentation boreholes were considered watertight except the extensometer borehole ALC4004 which was shown to be draining, in a similar way that the extensometer of the TED experiment. The annular space of the ALC1604 micro-tunnel was not backfilled; therefore, the cell was considered draining.

The COx THM parameters are the same as the values calibrated in the TED experiment. The casing is made of steel S235 with the following properties shown in Table 8. The teams were free to propose their own way of modeling the annular space.

The proper manner of representing this architecture was one of the main issues of this task. The teams were free to choose their own approach. In this way, the real geometry could be simplified (including or not the casing, applying a homogeneous thermal load on the rock wall

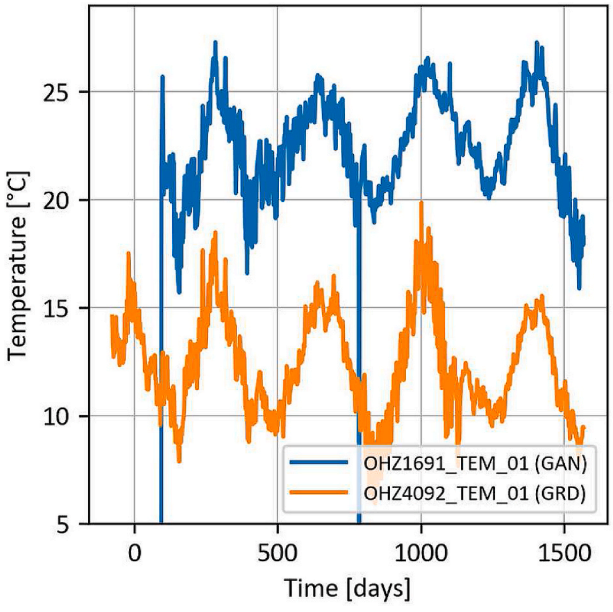

Fig. 13. Temporal evolution of the temperature on the GAN and the GRD drift walls.

Table 8
Properties of steel casing.

$E_{y,steel}$	ν_{steel}	λ_{steel}	ρ_{steel}	$C_{p,steel}$	α_{steel}
GPa	–	W/m/K	kg/m3	J/kg/K	1/K
210.0	0.3	54.0	7850	480	$1{\cdot}10^{-5}$

or not, modeling the annular space, etc.).

The numerical results were compared to the in-situ measurements at specific points in terms of temperature and pore pressure and their coordinates are given in Table 9. In order to capture well the anisotropic behavior of the COx, two points are located perpendicular and two other points are parallel to the bedding plane. All the points are located in the heated zone except one point that is located near the GAN drift wall (ALC1616_05).

6.2. Modeling approaches

The modeling teams kept their respective models along with the calibrated parameters in the TED experiment. Following the approach in the TED experiment, the thermal model was used to predict the temperature which was then compared to the provided measurements in the field; the heat input was reduced to 95% to account heat losses. The fully coupled THM formulation was used to predict the pore pressure and be compared against the pore pressure measurements and as a first approach, no EDZ around the micro-tunnel was considered.

Regarding the geometry, Andra and Quintessa did not model the steel casing or the annular space. NWMO modeled the steel casing but not the annular space, whereas UFZ/BGR and LBNL worked with a detailed geometry that took into account the casing and the annular space. The annular space was modeled with air properties during 400 days after the micro-tunnel excavation as explained in the experiment description. Then, the air properties were replaced by the rock properties. Andra and LBNL modeled a porous medium inside the borehole to simulate intermediate drained conditions with a permeability on the order of 10^{-15} m^2 as it was done for the TED experiment.

6.3. Results

The results of the blind prediction of the temperature and the pore pressure are presented from the beginning of the main heating phase until 1000 days after the beginning of the cell excavation (Figs. 14 and 15). The measurements are represented by circles and the numerical results by solid or dashed lines.

The numerical results of all modeling teams for the blind prediction show a good agreement with the measured temperature evolution (Fig. 14). The good prediction of the temperature at sensors located in the parallel and perpendicular direction to the bedding shows that the thermal conductivity coefficient and its respective anisotropic ratio were well calibrated. There is a maximum overestimation of 2 °C for the

Table 9
Measurement points for blind prediction of the ALC experiment.

Sensor	Direction to the bedding plane	Coordinates (x, y, z)	Type of measure
ALC1617_01	Perpendicular	(21.8, 0.72, 3.84)	Temperature and pressure
ALC1617_02	Perpendicular	(17.4, 0.57, 3.17)	Temperature and pressure
ALC1616_02	Parallel	(17.6, −2.42, 0.22)	Temperature and pressure
ALC1616_05	Parallel	(5.1, −2.78, 0.10)	Temperature and pressure
ALC4005_02	Intermediate	(13.0, 1.79, 2.79)	Temperature and pressure
ALC4005_04	Intermediate	(13.0, 7.18, 1.72)	Temperature and pressure

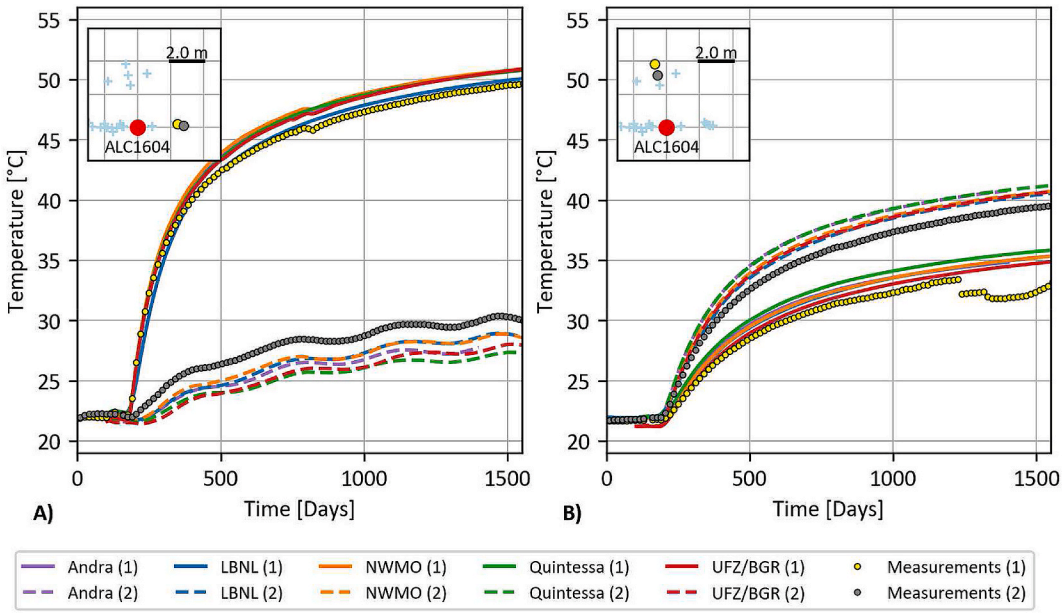

Fig. 14. Comparison of numerical prediction and measurements of temperature at sensors: (A) ALC1616_02 (1) and ALC1616_05 (2), located parallel to bedding and (B) ALC1617_01 (1) and ALC1617_02 (2), located perpendicular to bedding.

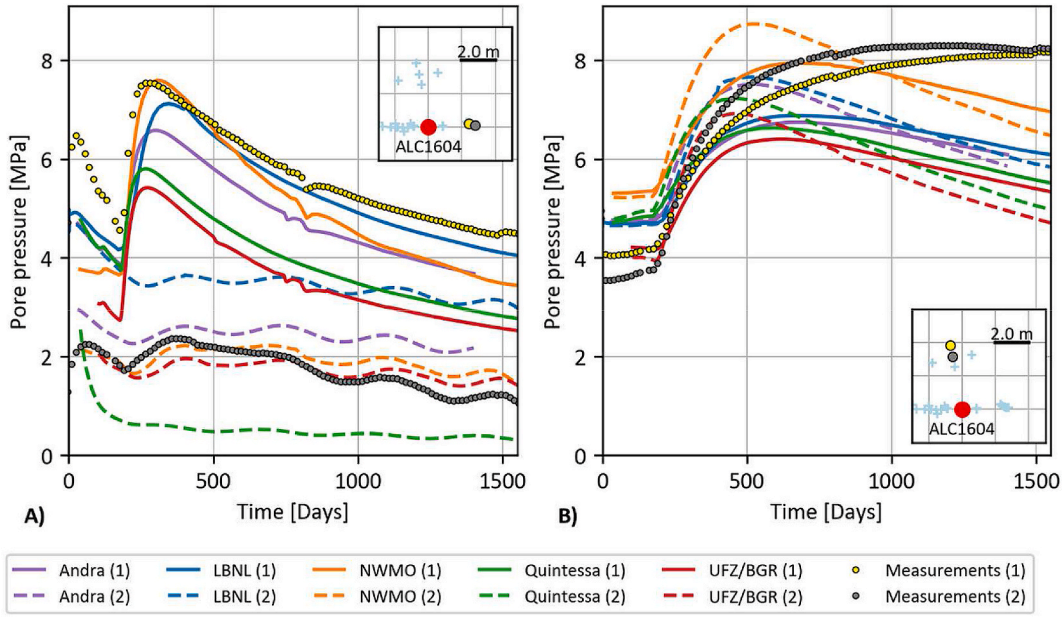

Fig. 15. Comparison of numerical prediction and measurements of pore pressure at sensors: (A) ALC1616_02 (1) and ALC1616_05 (2), located parallel to bedding and (B) ALC1617_01 (1) and ALC1617_02 (2), located perpendicular to bedding.

sensors located at the heated zone. On the contrary, an underestimation of the temperature is observed for most of the teams at the sensors located relatively far from the heated zone which may be essentially due to the fact that thermal convection and thermal radiation inside the micro-tunnel were neglected. Moreover, the choice of modeling the casing and the annular space seems to have a negligible effect on the temperature evolution at the measuring points.

The numerical results of the predicted pore pressure by the modeling teams are shown in Fig. 15. The pore pressure before the beginning of the main heating phase was not well captured in most of the cases and have not been shown on the Figures. However, some modeling teams not only captured the pore pressure evolution near the GAN drift wall due to the seasonal temperature variation but also globally, meaning that the modeling of the EDZ around the GAN drift was well approximated. In general, pore pressure build-up due to heating was well represented in the direction parallel to the bedding (i.e., ALC1616_02) as well as ALC4005_04. On the contrary, the measured pore pressure in the sensors located in the direction perpendicular to the bedding (i.e., ALC1617_01 and ALC1617_02) shows a lower dissipation which was not captured by any of the teams. This remains an open question of Task E modeling exercise and needs to be tackled again in future works as it could not be resolved currently even after intense discussion and various attempts as discussed in the following paragraph.

Further analyses have been performed by each team to obtain a better agreement with the pore pressure evolution observed in the field. Guo et al.,[37] study the possible convection and radiation effects in the

non-heated part of the micro-tunnel by assuming an equivalent thermal conduction coefficient. However, this approximation only improved the numerical results of the temperature in the non-heated part. Xu et al.,[39] performed a parametric analysis of Biot coefficient and permeability concluding that the Biot coefficient has a negligible impact on the trend of the pore pressure evolution whereas lower permeability values improve the pore pressure evolution in the direction perpendicular to the bedding. However, it worsens the numerical results in the direction parallel to the bedding. These results are also confirmed by Thatcher et al.,[40] that obtained a good agreement with the pore pressure evolution in the direction perpendicular to the bedding; the permeability values were one order of magnitude lower than those obtained for the TED experiment. This could be explained by the existence of lower permeability zones than the values obtained for the TED experiment. It is also worth mentioning that in the mentioned work,[40] the EDZ around the micro-tunnel was modeled with a higher permeability (isotropic equal $1{\cdot}10^{-18}$ m^2) and lower Young's modulus (isotropic equal 1 MPa). This may indicate that the modification of the mechanical-hydraulic properties can affect the THM response in the far field although the EDZ is limited in the vertical direction. According to Armand et al.,[28] the EDZ exhibits a larger extension in the horizontal direction when the cell is excavated along the major stress direction as it is the case of the ALC micro-tunnel. A possible explanation could be the pore pressure field around the cell prior to the heating stage as pointed out by Bumbieler et al.,.[2] The pore pressure measurements show lower values than the ones obtained by the numerical simulations. This difference could lead to different hydraulic gradients (i.e., the dissipation process may be accelerated in the numerical simulations). Better results have been obtained when using mechanical models that consider plasticity and time-dependent effects; the use of a time-dependent anisotropic elasto-plastic model[2] for the drilling of the micro-tunnel yielded a better description of the pore pressure field and consequently to a better reproduction of the pore pressure evolution during the heating phase.

Moreover, it is important to bear in mind that in the small-scale experiment the sensor locations were between 3 and 40 cell diameters away from the heating source; particularly, the sensors used for calibration of the pore pressure (TED1253_01 and TED1258_01) were located at approximately 7 cell diameters away from TED1201, whereas, in the ALC experiment, the sensor locations used for the blind prediction were approximately 3 cell diameters away from ALC1604. This means that, unlike the TED experiment where the measurement points were located in the far field, the measurement points of the ALC experiment were in a transition zone between the near and far field in which the modification of the hydro-mechanical properties may eventually have some influence on the pore pressure. Therefore, it would have been interesting to study how the pore pressure would evolve at points located at the same proportional distance of the measuring points in the TED experiment to have a better understanding of the THM behavior of the COx at the far field.

Even though the pore pressure trend was not captured in the direction perpendicular to bedding, the numerical results globally show a good prediction of the THM response of the COx with the parameters calibrated in the TED experiment using the thermo-poro-elastic approach.

7. Conclusions

This work was devoted to the study of the thermo-hydro-mechanical (THM) behavior of the Callovo-Oxfordian claystone (COx) at different scales by modeling two in-situ heating experiments at the Meuse/Haute-Marne Underground Research Laboratory (MHM URL): a small-scale experiment with three parallel cells of small diameter (TED) and a full-scale experiment of the 2009 French concept for one single HLW disposal cell (ALC).

First, a verification test (Step 1) guaranteed that the numerical codes reproduce the main THM processes by performing a 3D THM exercise and it was successfully passed by the modeling teams. This step was important not only to verify the teams' conceptual models against an analytical solution but also to evaluate more realistic expressions such as water properties that were not considered in the analytical solution. Since each team used slightly different expressions of equations of state, the numerical results lead to slight changes in the pore pressure.

Then, an interpretative modeling of the TED experiment was performed to calibrate the THM parameters of the COx (Step 2). The modeling teams chose the thermo-poro-elastic approach that had previously been verified in the validation test. The thermal parameters were well-calibrated as confirmed by the good fit of the numerical results and the temperature evolution observed at the different sensors. However, the calibration of the hydro-mechanical parameters required much more effort. One of the reasons was that the focus was on the heating experiment and not on the excavation of the gallery where the experiment was located, nor on the drilled boreholes; therefore, the initial pore pressure field was not well reproduced. The overall numerical results showed a good agreement with the measurements and the pore pressure build-up due to heating was well captured by all teams, mainly in the direction parallel to the bedding plane. The calibrated permeability was the parameter with the largest differences among the teams. The anisotropy ratio of the permeability was higher than the values measured in the field. The use of basic simplifications such as increasing the permeability around the gallery to represent the Excavation Damaged Zone and assuming a porous medium inside the boreholes to represent intermediate drained conditions proved to be reliable tools to better describe the conditions in which the heating experiment was performed.

Finally, the ALC experiment was blind predicted based on the model calibrations obtained in the TED experiment. The modeling teams kept their respective conceptual models. The blind prediction of the temperature showed an overestimation of less than 2 °C. It is important to mention that in most of the cases the steel casing and the initial gap at the vault between the steel casing and the rock were not represented. The pore pressure only was well predicted in the parallel direction to the bedding plane whereas the slow dissipation of the pore pressure in the direction perpendicular to the bedding plane was not captured by any of the teams – which remains an open question of the present study.

The main objective of this work was to study how the conceptual models proposed by the modeling teams along with the calibrated parameters obtained from the modeling of the small-scale experiment would predict a full-scale experiment. The numerical results showed a good prediction of the temperature and the pore pressure even with the models that did not represent the casing and/or the gap between the casing and the rock and no important scale effects were observed in the far field between TED and ALC experiments.

Finally, it is also important to mention that thermo-poro-elastic modeling has been able to represent the global behavior of the TED and ALC experiments and has proved to be a reliable tool for the prediction of the THM response of the COx in the far field which could be useful when modeling a large-scale deep geological repository, where one of the main focus is to calculate the required distance between two parallel High Level Waste cells. It is worth mentioning that thermo-poro-elastic models cannot represent the THM behavior of the rock in the vicinity of the cells, where the non-linarites due to the presence of the fractures and damage dominate the THM response. The last step of DECOVALEX-2019 Task E, performing reliable large-scale analysis of high-level radioactive repositories, is addressed in Ref.[41]

Declaration of competing interest

The authors declare that they have no known competing financial interests or personal relationships that could have appeared to influence the work reported in this paper.

Acknowledgements

DECOVALEX is an international research project comprising participants from industry, government and academia, focusing on development of understanding, models and codes in complex coupled problems in sub-surface geological and engineering applications; DECOVALEX-2019 is the current phase of the project. The authors appreciate and thank the DECOVALEX-2019 Funding Organizations Andra, BGR/UFZ, CNSC, US DOE, ENSI, JAEA, IRSN, KAERI, NWMO, RWM, SÚRAO, SSM and Taipower for their financial and technical support of the work described in this report. The statements made in the report are, however, solely those of the authors and do not necessarily reflect those of the Funding Organizations.

The ALC1604 experiment presented in this article has received funding from the European Atomic Energy Community's Seventh Framework Program under Grant Agreement n◦269905, the LUCOEX project. The financial support is gratefully acknowledged.

Funding for LBNL's modeling work was provided by the Spent Fuel and Waste Science and Technology, Office of Nuclear Energy, of the U.S. Department of Energy under Contract Number DE-AC02-05CH11231 with Lawrence Berkeley National Laboratory.

Funding for Quintessa's modeling work was provided by Radioactive Waste Management Ltd.

UFZ/BGR teams work was supported by funding from the Federal Institute for Geosciences and Natural Resources (grant number 204–10088620) and within the iCROSS project (Integrity of nuclear waste repository systems – Cross-scale system understanding and analysis) funded by the Federal Ministry for Education and Research (BMBF) and the Helmholtz Association (grant numbers 02NUK053E, SO-093).

The various funding for conducting research work for DECOVALEX-2019 Task E is greatly acknowledged.

References

1 Armand G, Bumbieler F, Conil N, de La Vaissière R, Bosgiraud J-M, Vu M-N. Main outcomes from in situ thermo-hydro-mechanical experiments programme to demonstrate feasibility of radioactive high-level waste disposal in the Callovo-Oxfordian claystone. *J. Rock Mech. Geotech. Eng.* 2017;9(3):415–427. https://doi.org/10.1016/j.jrmge.2017.03.004.

2 Bumbieler F, Plúa C, Tourchi S, et al. Feasibility of constructing a full-scale radioactive high-level waste disposal cell and characterization of its thermo-hydro-mechanical behavior. Int J Rock Mech Min Sci. 2021;137:104555. https://doi:10.1016/j.ijrmms.2020.104555.

3 Necib S, Linard Y, Crusset D, et al. Corrosion at the carbon steel-clay borehole water and gas interfaces at 85°C under anoxic and transient acidic conditions. *Corrosion Sci.* 2016;111:242–258. https://doi.org/10.1016/j.corsci.2016.04.039.

4 Vu M-N, Seyedi D, Armand G. Thermo-poro-mechanical coupled processes during thermal pressurization around nuclear waste repository. In: *VI International Conference on Computational Methods for Coupled Problems in Science and Engineering. Venice*. 18-20 May 2015.

5 Darius Seyedi, Gilles Armand, Nathalie Conil, Manon Vitel, Minh-Ngoc Vu. On the thermo-hydro-mechanical pressurization in Callovo-Oxfordian claystone under thermal loading. In: *Sixth Biot Conference on Poromechanics*. 9-13 July 2017:754–761. https://doi.org/10.1061/9780784480779.093.

6 Wileveau Y, Su K, Ghoreychi M. A heating experiment in the argillites in the Meuse/Haute-Marne Underground research laboratory. In: *The 11th International Conference on Environmental Remediation and Radioactive Waste Management*. Bruges; 2-6 September 2007:939–944. https://doi.org/10.1115/ICEM2007-7276.

7 Conil N, Vitel M, Plua C, Vu MN, Seyedi D, Armand G. In situ investigation of the THM behavior of the Callovo-Oxfordian claystone. *Rock Mech Rock Eng.* 2020;53(6):2747–2769. https://doi.org/10.1007/s00603-020-02073-8.

8 Gens A, Sánchez M, Guimarães LDN, et al. A full-scale in situ heating test for high-level nuclear waste disposal: observations, analysis and interpretation. *Geotechnique.* 2009;59(4):377–399.

9 Dizier A, Chen G, Li XL, Rypens J. The PRACLAY heater test after two years of the stationary phase. *ESV Euridice*. 2017:64.

10 Bossart P, Jaeggi D, Nussbaum C. Experiments on thermo-hydro-mechanical behaviour of Opalinus clay at Mont Terri rock laboratory, Switzerland. *J. Rock Mech. Geotech. Eng.* 2017;9(3):502–510. https://doi.org/10.1016/j.jrmge.2016.11.014.

11 Jia Y, Bian HB, Duveau G, Su K, Shao JF. Numerical modelling of in situ behaviour of the Callovo–Oxfordian argillite subjected to the thermal loading. *Eng Geol.* 2009;109(3):262–272. https://doi.org/10.1016/j.enggeo.2009.08.012.

12 Jobmann Michael, Li Sha, Polster Mirko, Breustedt Michael, Schlegel Roger, Vymlatil Petr, et al. Using statistical methods for rock parameter identification to analyse the THM behaviour of Callovo-Oxfordian claystone due to heating. *J Geol Resour Eng.* 2016;4(3). https://doi.org/10.17265/2328-2193/2016.03.003.

13 Garitte B, Nguyen TS, Barnichon JD, et al. Modelling the Mont Terri HE-D experiment for the Thermal–Hydraulic–Mechanical response of a bedded argillaceous formation to heating. *Environ Earth Sci.* 2017;76(9):345. https://doi.org/10.1007/s12665-017-6662-1.

14 Booker JR, Savvidou C. Consolidation around a point heat source. *Int J Numer Anal Methods GeoMech.* 1985;9(2):173–184. https://doi.org/10.1002/nag.1610090206.

15 Chaudhry AA, Buchwald J, Kolditz O, Nagel T. Consolidation around a point heat source (correction and verification). *Int J Numer Anal Methods GeoMech.* 2019. https://doi.org/10.1002/nag.2998.

16 COMSOL Multiphysics®. Www.Comsol.Com.

17 Code_aster. https://Code-Aster.Org/. (EDF R&D).

18 Rutqvist J, Wu Y-S, Tsang C-F, Bodvarsson G. A modeling approach for analysis of coupled multiphase fluid flow, heat transfer, and deformation in fractured porous rock. *Int J Rock Mech Min Sci.* 2002;39(4):429–442. https://doi.org/10.1016/S1365-1609(02)00022-9.

19 Rutqvist J. An overview of TOUGH-based geomechanics models. *Comput Geosci.* 2017;108:56–63. https://doi.org/10.1016/j.cageo.2016.09.007.

20 Maul P. *QPAC: Quintessa's General-Purpose Modelling Software*. Quintessa; 2013.

21 Wang W, Kolditz O. Object-oriented finite element analysis of thermo-hydro-mechanical (THM) problems in porous media. *Int J Numer Methods Eng.* 2007;69(1):162–201. https://doi.org/10.1002/nme.1770.

22 Kolditz O, Bauer S, Bilke L, et al. OpenGeoSys: an open-source initiative for numerical simulation of thermo-hydro-mechanical/chemical (THM/C) processes in porous media. *Environ Earth Sci.* 2012;67(2):589–599. https://doi.org/10.1007/s12665-012-1546-x.

23 Song Y, Davy CA, Bertier P, Troadec D. Understanding fluid transport through claystones from their 3D nanoscopic pore network. *Microporous Mesoporous Mater.* 2016;228:64–85. https://doi.org/10.1016/j.micromeso.2016.03.023.

24 Robinet J-C, Sardini P, Coelho D, et al. Effects of mineral distribution at mesoscopic scale on solute diffusion in a clay-rich rock: example of the Callovo-Oxfordian mudstone (Bure, France). *Water Resour Res.* 2012;48. https://doi.org/10.1029/2011WR011352.

25 Armand G, Conil N, Talandier J, Seyedi DM. Fundamental aspects of the hydromechanical behaviour of Callovo-Oxfordian claystone: from experimental studies to model calibration and validation. *Comput Geotech.* 2017;85:277–286. https://doi.org/10.1016/j.compgeo.2016.06.003.

26 Wileveau Y, Cornet FH, Desroches J, Blumling P. Complete in situ stress determination in an argillite sedimentary formation. *Phys Chem Earth, Parts A/B/C.* 2007;32(8-14):866–878. https://doi.org/10.1016/j.pce.2006.03.018.

27 Armand G, Noiret A, Zghondi J, Seyedi DM. Short- and long-term behaviors of drifts in the Callovo-Oxfordian claystone at the Meuse/Haute-Marne Underground research laboratory. *J. Rock Mech. Geotech. Eng.* 2013;5(3):221–230. https://doi.org/10.1016/j.jrmge.2013.05.005.

28 Armand G, Leveau F, Nussbaum C, et al. Geometry and properties of the excavation-induced fractures at the Meuse/Haute-Marne URL drifts. *Rock Mech Rock Eng.* 2014;47(1):21–41. https://doi.org/10.1007/s00603-012-0339-6.

29 Gens A, Vaunat J, Garitte B, Wileveau Y. In situ behaviour of a stiff layered clay subject to thermal loading: observations and interpretation. *Geotechnique.* 2007;57(2):207–228. https://doi.org/10.1680/geot.2007.57.2.207.

30 Coussy O. *Poromechanics*. second ed. Wiley; 2004.

31 Belmokhtar M, Delage P, Tang A-M, Menaceur H, Conil N. Poroelasticity of the Callovo–Oxfordian claystone. *Rock Mech Rock Eng.* 2016. https://doi.org/10.1007/s00603-016-1137-3.

32 Braun P, Ghabezloo S, Delage P, Sulem J, Conil N. Transversely isotropic poroelastic behaviour of the Callovo-Oxfordian claystone: a set of stress-dependent parameters. *Rock Mech Rock Eng.* 2020. https://doi.org/10.1007/s00603-020-02268-z.

33 Rowe AM, Chou JCS. Pressure-volume-temperature-concentration relation of aqueous sodium chloride solutions. *J Chem Eng Data.* 1970;15(1):61–66. https://doi.org/10.1021/je60044a016.

34 Sharqawy MH, Lienhard JH, Zubair SM. Thermophysical properties of seawater: a review of existing correlations and data. *Desalination Water Treat.* 2010;16(1-3):354–380.

35 Muller AB, Pearson FJ, Finley NC. *Intera Environmental Consultants., Sandia National Laboratories., U.S. Nuclear Regulatory Commission. Geochemical Parameters Used in the Bedded Salt Reference Repository, Risk Assessment Methodology. The Commission: Available from GPO Sales Program, Division of Technical Information and Document Control, U.S. Nuclear Regulatory Commission; National Technical Information Service*; 1981. https://catalog.hathitrust.org/Record/102603618. Accessed April 16, 2020.

36 Andrade ENDC. The viscosity of liquids. *Nature.* 1930;125(3148):309–310. https://doi.org/10.1038/125309b0.

37 Guo R, Thatcher KE, Seyedi DM, Plúa C. Calibration of the thermo-hydro-mechanical parameters of the Callovo-Oxfordian claystone and the modelling of the ALC experiment. *Int J Rock Mech Min Sci.* 2020;132:104351. https://doi.org/10.1016/j.ijrmms.2020.104351.

38 Wang W, Shao H, Nagel T, Kolditz O. Numerical simulation of coupled thermo-hydro-mechanical processes in heater experiments for nuclear waste disposal in Callovo-Oxfordian clay rock: Part 1: analysis of the small-scale heater experiment (TED). Int J Rock Mech Min Sci submitted for publication.

39 Xu H, Rutqvist J, Plúa C, Armand G, Birkholzer J. Modeling of thermal pressurization in tight claystone using sequential THM coupling: benchmarking and validation

against in-situ heating experiments in COx claystone. *Tunn Undergr Space Technol*. 2020;103:103428. https://doi.org/10.1016/j.tust.2020.103428.

40 Thatcher KE, Bond AE, Norris S, et al. Pore pressure response to disposal of heat generating radioactive waste in a low permeability host rock. *Int J Rock Mech Min Sci*. 2020;135:104456. https://doi.org/10.1016/j.ijrmms.2020.104456.

41 Plúa C, Vu MN, Armand G, et al. A reliable numerical analysis for large-scale modelling of a high-level radioactive waste repository in the Callovo-Oxfordian claystone. *Int J Rock Mech Min Sci.* 2021;140:104574. https://doi.org/10.1016/j.ijrmms.2020.104574.